Extracting the kinetic freeze-out properties of high energy pp collisions at the LHC with event shape classifiers*

Jialin He (何佳林)[1] Xinye Peng (彭忻烨)[1,2] Zhongbao Yin (殷中宝)[2] Liang Zheng (郑亮)[1,2,3†]

[1]School of Mathematics and Physics, China University of Geosciences (Wuhan), Wuhan 430074, China
[2]Key Laboratory of Quark and Lepton Physics (MOE) and Institute of Particle Physics, Central China Normal University, Wuhan 430079, China
[3]Shanghai Research Center for Theoretical Nuclear Physics, NSFC and Fudan University, Shanghai 200438, China

Abstract: Event shape measurements are crucial for understanding the underlying event and multiple-parton interactions (MPIs) in high energy proton-proton (pp) collisions. In this study, the Tsallis blast-wave model with independent non-extensive parameters for mesons and baryons was applied to analyze the transverse momentum spectra of charged pions, kaons, and protons in pp collision events at $\sqrt{s} = 13$ TeV classified by event shape estimators such as relative transverse event activity, unweighted transverse spherocity, and flattenicity. Our analysis reveals consistent trends in the kinetic freeze-out temperature and non-extensive parameter across different collision systems and event shape classes. The use of diverse event-shape observables in pp collisions has significantly expanded the accessible freeze-out parameter space, enabling a more comprehensive exploration of its boundaries. Among these event shape classifiers, flattenicity emerges as a unique observable for disentangling hard process contributions from additive MPI effects, which helps isolate collective motion effects encoded by the radial flow velocity. Through the analysis of the interplay between event-shape measurements and kinetic freeze-out properties, we gain deeper insights into mechanisms responsible for flow-like signatures in pp collisions.

Keywords: blast-wave model, tsallis statistics, pp collisions, event shape, kinetic freeze-out

DOI: 10.1088/1674-1137/ae07ba **CSTR:** 32044.14.ChinesePhysicsC.50014108

I. INTRODUCTION

Lattice quantum chromodynamics (QCD) calculations indicate that regions of extremely high energy density are likely to be created in high energy heavy ion collisions [1, 2]. In these regions, quarks and gluons confined in nucleons can be released, thereby forming a nearly perfect quark-gluon plasma (QGP) with high temperature and small viscosity [3]. The thermalization of deconfined nuclear matter occurs on an extremely short timescale and rapidly expands via the hydrodynamic evolution process [4, 5]. During the expansion of the QGP medium, the temperature of the system drops to a level where the quark and gluon degrees of freedom begin to freeze and form final-state hadrons [6]. The significant collective motion of the QGP matter during hydrodynamic evolution can lead to sizable collectivity effects in experiments embedded in the final state hadron momentum distributions. Analyzing the experimentally observed collective flow behavior of final-state hadrons provides valuable information about the evolution and phase transitions of QGP matter [7−11].

Recent observations of collective flow-like behaviors in small collision systems such as high-multiplicity proton-proton (pp) events have generated considerable discussion regarding the potential formation of QGP matter in these collisions where genuine fluid-like dynamics are unexpected [12−14]. It is speculated that hot spots arising from high initial energy density in small systems may induce sizable collective flow and strong temperature fluctuations. In pp collisions, the formation of these hot spots is believed to be linked to multiple-parton interactions (MPIs), defined as the occurrence of multiple independent partonic scatterings within a single hadronic collision [15]. This process contributes significantly to the underlying event by enhancing particle multiplicity and energy deposition in localized regions. The cumulative effects of MPI can create conditions resembling those seen in lar-

Received 28 May 2025; Accepted 15 September 2025; Published online 16 September 2025

* Supported by the National Key Research and Development Program of China (2024YFA1610800), the National Natural Science Foundation of China (12205259, 12147101, 12275103, 12061141008), the Fundamental Research Funds for the Central Universities, China University of Geosciences(Wuhan) with G1323523064 and the Innovation Fund of Key Laboratory of Quark and Lepton Physics QLPL2025P01

† E-mail: zhengliang@cug.edu.cn

ger collision systems [16]. High MPI activity leads to denser particle environments and the isotropization of particle distributions caused by the superposition of multiple scatterings that can amplify final-state interactions or mimic azimuthal anisotropies traditionally associated with hydrodynamic flow.

Experimentally constraining MPI effects is vital for disentangling their contributions from genuine collective flow and other non-flow correlations in the final state. The number of charged particles within certain detector acceptance region are initially proposed to study the MPI dependent effects and used to compare flow signals across different collision systems. However, this observable is found to bias the high multiplicity jets in the corresponding detector region [17, 18]. Measurements of event shape observables for small systems such as transverse event activity [19, 20], spherocity [21, 22], and charged particle flattenicity [23, 24] have been proposed to identify events with less bias to jet productions but more sensitive to the MPI related contributions. By correlating these event shape observables with flow-sensitive measurements, such as the elliptic flow coefficient and long-range correlations, experimental collaborations have begun to quantify the extent to which MPIs shape the observed signals [25−27].

In this study, we extract the kinetic freeze-out temperature and radial flow velocity of collision systems via applying the Tsallis blast-wave (TBW) analysis [28, 29] to the transverse momentum spectra in high energy pp collision events with different event shape classifiers. The imprints of the initial fluctuations and viscosity of the expanding medium can be embedded in the non-extensive parameter in the TBW model and its correlation with temperature and flow velocity [30−34]. By systematically comparing the freeze-out parameters extracted using various event shape classifiers, we directly assess their effectiveness in event shape engineering and their sensitivity to isolate the underlying collective dynamics for small systems. The non-extensive parameter, which characterizes deviations from local thermal equilibrium, is expected to decrease in more isotropic and MPI dominated events, reflecting a system closer to thermalization. In contrast, jet dominated events are expected to exhibit enhanced non-equilibrium features and reduced collective flow signatures. Through this comparative analysis, we aim to determine the extent to which each event shape observable can disentangle soft, flow like behavior from contributions associated with hard scattering processes. Comparing the extracted parameters from different event shape variables is important to understand the sensitivity of these event shape control variables to the underlying collective dynamics in pp collisions [35]. Exploring the kinetic freeze-out features varying with event shapes can significantly aid in quantifying the MPI effect when generating the flow like effects in small systems and help with the understanding of the origin of the collectivity like behavior observed in small systems.

The rest of this paper is organized as follows. Section II briefly describes the event shape classifiers used in this analysis and the key parameters in our TBW fit framework. Section III compares the extracted freeze-out properties for different event shapes, and Sec. IV summarizes the main conclusions.

II. RESEARCH APPROACH

A. Relative transverse event activity

Event activity measurements are indispensable for probing the underlying event properties and understanding MPI effects in high-energy proton-proton collisions. These effects are usually studied by analyzing the particle production in azimuthal regions relative to the leading particle direction in one event. With the trigger particle being the one with the largest p_T in an event and the rest termed as associated particles, the azimuthal plane can be divided into three different topological regions defined by the angular difference ($|\Delta\phi| = |\phi_{\rm trig} - \phi_{\rm assoc}|$) between the trigger and the associate particle [20, 36]. The toward region $|\Delta\phi| < 60^\circ$ is expected to be associated with the main jet production in an event; the away region $|\Delta\phi| \geq 120^\circ$ contains particles fragmented from the recoil jet; and the particles in the transverse region $60^\circ \leq |\Delta\phi| < 120^\circ$ predominantly come from the underlying event process, which are subject to various sources beyond jet fragmentation, including initial- and final-state radiation, beam remnants, and MPIs [37]. Therefore, the relative transverse activity (R_T) [19] built from the transverse region that is expected to have low sensitivity to the hard processes is proposed to classify events and gain insight into the modifications to the charged hadron p_T spectra

$$R_T = N_T / \langle N_T \rangle, \tag{1}$$

where N_T represents the number of charged particles measured in the transverse region for each event, and $\langle N_T \rangle$ represents the average number of charged particles across all analyzed events. The experimental data used in this study divide R_T into four intervals: 0−0.5, 0.5−1.5, 1.5−2.5, and 2.5−5 [20]. Events are selected by requiring a leading charged particle with $p_T > 5$ GeV/c at mid-rapidity. The transverse momentum spectra of identified hadrons are analyzed separately in the toward, away, and transverse regions, defined relative to the azimuthal angle of the leading particle. Increasing R_T represents a transition to the multiparton interaction dominated underlying event categories.

B. Unweighted transverse spherocity

In high-energy hadronic collisions, spherocity is a key

event-shape observable used to characterize the geometrical shapes of particle distributions in the transverse plane [21]. Spherocity distinguishes between jet-like events featuring collimated, high-momentum particle productions, and isotropic events, where particles are uniformly distributed signaling softer processes. Unlike the sphericity measurement [22], which assesses three-dimensional isotropy and is more suitable for e^+e^- collisions, spherocity is well-suited to hadron colliders, wherein the transverse momentum information is of great interest. In the traditional spherocity calculation [23], tracks with high p_T contribute disproportionately, leading to significant differences between neutral and charged particles in jet-like events. This study focuses on unweighted transverse spherocity, where all particles contribute equally, regardless of their transverse momentum. By suppressing jet contributions, unweighted spherocity enhances sensitivity to soft and bulk particle production. Such an approach is effective in small systems, where separating jet-induced events from those potentially exhibiting collective behavior is crucial. We employ the p_T data provided in Ref. [26], categorized by the unweighted transverse spherocity estimator ($S_O^{p_T=1}$). It is calculated as

$$S_O^{p_T=1} = \frac{\pi^2}{4} \min_{\hat{n}} \left(\frac{\sum_i |\hat{p}_{T,i} \times \hat{n}|}{N_{\rm trks}} \right)^2, \tag{2}$$

where the summation is over all charged particles with transverse momentum $p_T > 0.15$ GeV/c. $\hat{p}_T$ represents the unit vector of transverse momentum, $N_{\rm trks}$ represents the number of charged particles in a given event, and $\hat{n}$ represents the unit vector that minimizes $S_O^{p_T=1}$. This $S_O^{p_T=1}$ definition treats all charged tracks with equal weight, setting $p_T = 1$ for each, in contrast to the original transvserse momentum weighted spherocity formulation. To constrain the hardness of the events more effectively, the unweighted spherocity data [26] used in this study is obtained using a mid-rapidity multiplicity estimator in tandem with $S_O^{p_T=1}$ selection divided into three categories: 0−10%, 90%− 100%, and 0−100% ($S_O^{p_T=1}$-integrated). The 0−10% interval indicates low spherocity values corresponding to jet-like events with particles predominantly aligned in the azimuthal plane, and the 90−100% interval denotes high spherocity values associated with isotropic events where particles are uniformly distributed in the azimuthal plane. Only high multiplicity events in the top 1% mid-rapidity multiplicity percentile are used in these data.

C. Flattenicity

Flattenicity is a new event-shape observable developed by ALICE Collaboration to measure local charged-particle multiplicity fluctuations in the forward V0 detector on an event-by-event basis [23]. Unlike traditional multiplicity estimators, which focus on total yield and can be biased by multi-jet events, flattenicity targets density variations without momentum weighting, reducing bias from high p_T jets and enhancing sensitivity to soft particle production [24]. The flattenicity measurement obtained by ALICE is performed using the forward V0 scintillator arrays [38], wherein the distribution of charged-particle multiplicities across the pseudorapidity (η) and azimuthal angle (ϕ) phase space are segmented into $N_{\rm cell} = 64$ elementary cells. The flattenicity (ρ) is defined as

$$\rho = \frac{\sqrt{\sum_{i=1}^{64} \left(N_{\rm ch}^{{\rm cell},i} - \langle N_{\rm ch}^{\rm cell} \rangle \right)^2 / N_{\rm cell}^2}}{\langle N_{\rm ch}^{\rm cell} \rangle}, \tag{3}$$

where $N_{\rm ch}^{{\rm cell},i}$ and $\langle N_{\rm ch}^{\rm cell} \rangle$ represent the particle multiplicity in the cell and average multiplicity across all 64 cells in each event, respectively. This formula quantifies how evenly particles are distributed across η-ϕ cells. A small ρ value indicates a uniform multiplicity distribution, suggesting isotropic particle production, while a large ρ value points to significant fluctuations, possibly because of clustered activity such as jets or hard processes. Comparisons with PYTHIA Monte Carlo models indicate that flattenicity correlates with the number of multiparton interactions and behaves differently compared to those of traditional V0M multiplicity estimators, which makes it a powerful tool for disentangling MPI-driven fluctuations from collective phenomena. In experiments, the results are commonly expressed in terms of $1-\rho$ so that higher values correspond to more isotropic events, thereby aligning the orientation of flattenicity with the conventions of other event-shape observables. The distribution of $1-\rho$ is then divided into several percentile intervals with the lowest percentile (*e.g.* 0−1%) capturing the flattest events with maximal MPIs, whereas the highest percentile (*e.g.* 50−100%) selects the bumpy events with few MPIs, providing a uniform framework that mitigates biases from hard scattering when studying soft QCD dynamics.

Our current study employs the data from Ref. [39], wherein a double-differential event classification based on both multiplicity and flattenicity is applied. We include the p_T spectra from both the minimum bias sample, which encompasses all inelastic collisions (V0M percentile 0−100%), and from the high multiplicity bin, which consists of the top 1% of events with the highest multiplicity (V0M percentile 0−1%). Within each category, events are classified according to their flattenicity values. This approach enables us to explore the multiplicity-dependent nature of flattenicity across a broad spectrum of event types, thereby offering insights into the dynamics of high-energy collisions.

D. Tsallis blast-wave model

In the TBW model, an invariant differential yield is obtained by integrating a Tsallis-distributed source over longitudinal rapidity, azimuthal angle, and transverse radius, combining collective expansion with non-extensive statistics for describing the full p_T spectrum in high-energy collisions. The invariant differential particle yield of a hadron with mass m within the TBW framework can be expressed as

$$\begin{aligned}\frac{\mathrm{d}^2N}{2\pi m_T \mathrm{d}m_T \mathrm{d}y}\Big|_{y=0} = A\int_{-y_b}^{+y_b} m_T\cosh(y_s)\mathrm{d}y_s\int_{-\pi}^{\pi}\mathrm{d}\phi \\ \times\int_0^R r\mathrm{d}r\left[1+\frac{q-1}{T}(m_T\cosh(y_s)\cosh(\rho)\right. \\ \left. - p_T\sinh(\rho)\cos(\phi))\right]^{-1/(q-1)}.\end{aligned} \tag{4}$$

where T, R, and A represent the freeze-out temperature of the expanding source, boundary along the transverse radial direction (edge of the hard sphere), and normalization constant, respectively. $m_T = \sqrt{p_T^2+m^2}$ represents the transverse mass of the particle, y_s represents the rapidity of the source, y_b represents the beam rapidity, and ϕ represents the angle of particle emission relative to the fluid flow velocity. Further, $\rho = \tanh^{-1}\beta(r)$ defines the radial flow profile, described by the transverse flow $\beta(r) = \beta_S\left(\frac{r}{R}\right)^n$, where n represents the flow profile index. $\langle\beta\rangle = \beta_S\cdot 2/2+n$ represents the average transverse flow velocity. Setting n = 1 yields a linear velocity profile, resulting in $\langle\beta\rangle = 2/3\beta_S$ [29]. To account for blue - shift effects caused by collective expansion, an effective temperature $T_{\mathrm{eff}} = \sqrt{\frac{1+\langle\beta\rangle}{1-\langle\beta\rangle}}T$, which reflects the observed p_T spectra hardening, is often introduced. In the TBW4 variant, the TBW model is extended by introducing independent non - extensivity parameters q_M for mesons and q_B for baryons [28, 40]. This modification yields a markedly improved fit to identified hadron p_T spectra in small collision systems [29, 33]. This performance enhancement underscores the pivotal role of baryon - number–dependent non - equilibrium dynamics in small systems, where fragmentation and collective effects interplay in unique ways. In this study, we perform the blast-wave analysis of the p_T spectra of pions, kaons, and protons at mid-rapidity in pp collisions with different event shapes using the TBW4 fit. Restricting the analysis to these particles enables a more controlled and meaningful extraction of the bulk freeze-out dynamics. In the end, we would like to emphasize that the use of the TBW model in this work provides a flexible yet phenomenological framework to characterize freeze-out properties in small systems. Although the TBW model captures key features of the transverse momentum spectra, it lacks a microscopic foundation and assumes radial symmetry in both the velocity and temperature fields of the expanding source, which might be a simplification especially for the strongly fluctuating asymmetric dynamics present in individual pp collisions dominated by jets. The extracted parameters should therefore be interpreted as effective quantities that reflect the combined effects of thermal motion, radial flow, and non-equilibrium fluctuations. These limitations will motivate future work incorporating more differential modeling with microscopic evolution mechanism and experimental correlation analyses [41].

III. RESULTS

A. Transverse momentum spectra

This section compares the TBW model fits considering independent baryon and meson non-extensive parameters of transverse momentum spectra for charged pions, kaons, and protons in pp collisions at $\sqrt{s}$ = 13 TeV using different event shape classifiers. We only include transverse momentum data within the $p_T < 3$ GeV/c region in our analysis to ensure consistent bulk property extraction. The average flow velocity is constrained to $0 < \langle\beta\rangle < 2/3$ for eliminating the non-physical parameter regime. We calculate the pull distribution defined as *pull*=(*fit-data*)/(*data error*) to quantify deviations between model fits and experimental data. Positive (negative) values indicate where the fit overestimates (underestimates) the data. The pull magnitude directly corresponds to the number of standard deviations between the fit and experimental measurements.

In Fig. 1, we present the comparison of TBW4 fits to the p_T spectra data [20] divided into different event topology regions, constrained by the transverse event activity R_T in each region. Events used in this analysis are selected by requiring a leading charged particle with $p_T > 5$ GeV/c at mid-rapidity. The event topology regions are defined relative to the azimuthal angle of this leading particle. The results are displayed in panels organized from left to right as the toward, away, and transverse regions. From top to bottom, the panels correspond to R_T intervals of 0−0.5, 0.5−1.5, 1.5−2.5, and 2.5−5. Experimental data points and theoretical fits are represented by markers and curves respectively, where black, red, and blue colors correspond to pions, kaons, and protons. The $\chi^2/nDOF$ values obtained from each fit are indicated within the panels, with further details of the fit parameters provided in Table 1.

As shown in Fig. 1, the features of the particle yield dependent on the event topology region and R_T variation are well reproduced in TBW4 fits. Considering that these particle p_T spectra are selected by requiring at least a

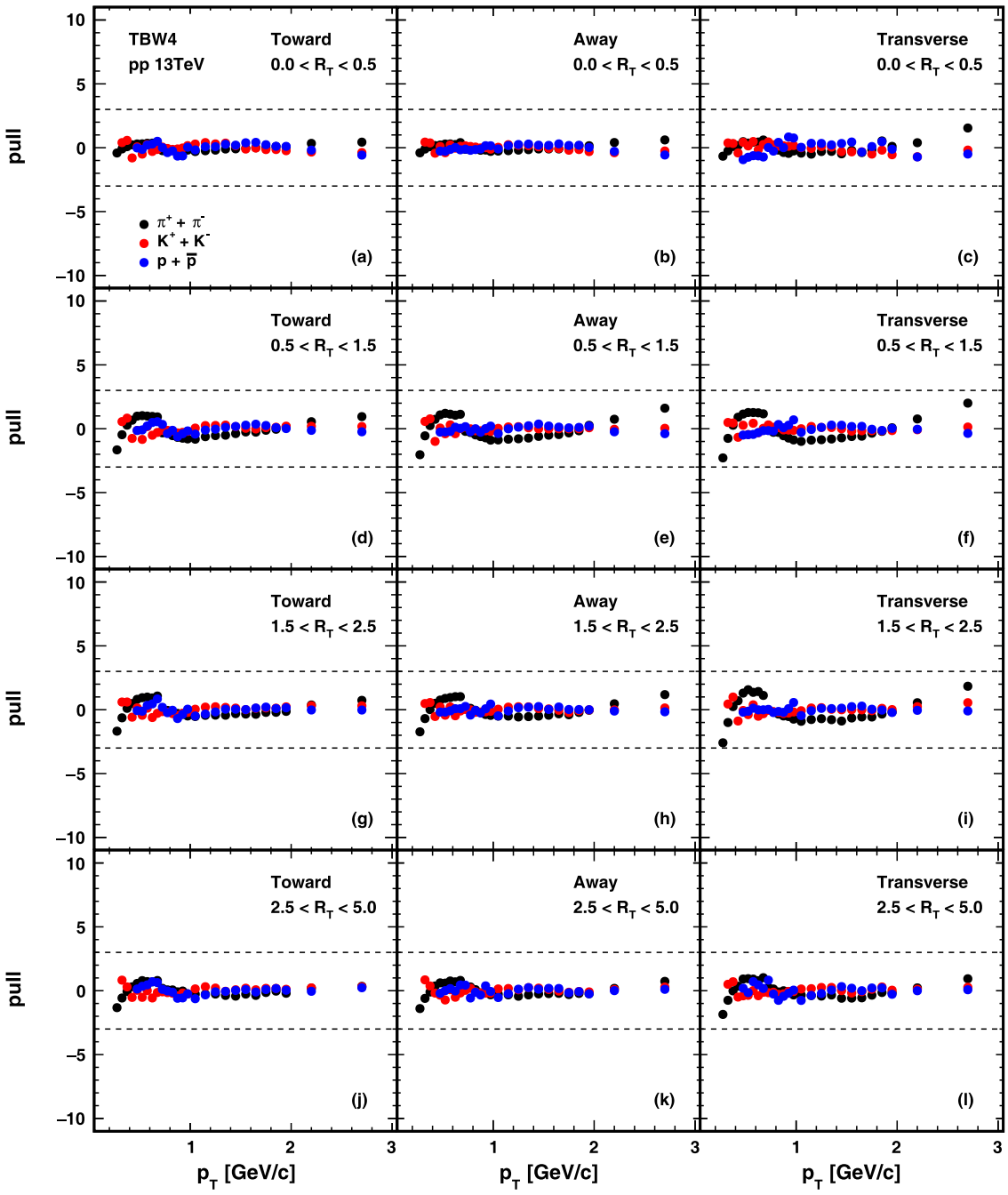

Fig. 1. (color online) TBW4 fits to hadron spectra in pp collisions at $\sqrt{s}$ = 13 TeV. Black, red, and blue correspond to π, K, and p particles, respectively. The points represent the ALICE experimental data [20], and the lines represent the fit results. From top to bottom, the rows represent R_T intervals of 0−0.5, 0.5−1.5, 1.5−2.5, and 2.5−5. From left to right, the columns represent the forward, backward, and transverse regions. The uncertainties in experimental data are the quadratic sum of statistical and systematic errors.

trigger particle with $p_T > 5$ GeV/c in the event, it is interesting to see that TBW4 fit still works well for all these different topological regions. The comparison reveals that the particle yield increases with R_T in all topological regions. In the low R_T bin such as 0−0.5, the particle yield in the toward and away regions is higher than that in the transverse region, indicating that the event is jet dominant. In high R_T events with R_T around 2.5−5.0, the particle yield in the transverse region is significantly greater than that in the other two regions, indicating that the jet effect weakens, and softer processes such as partonic interactions become more important. In all R_T bins, the p_T spectra in the toward and away regions are always harder than the transverse region p_T spectra for different particle species. This difference indicates that the toward and away regions are more sensitive to jet productions in

Table 1. Extracted kinetic freeze-out parameters and $\chi^2/nDoF$ from TBW4 fits to identified particle transverse spectra in pp collisions at $\sqrt{s}$ = 13 TeV for different regions and R_T values.

Region	R_T	$\langle\beta\rangle$	T/MeV	q_M-1	q_B-1	$\chi^2/nDoF$
Toward	0.0< R_T <0.5	0.285±0.056	56±9	0.209±0.007	0.177±0.008	7/68
	0.5< R_T <1.5	0.378±0.022	53±3	0.197±0.004	0.166±0.006	19/68
	1.5< R_T <2.5	0.448±0.018	56±4	0.184±0.005	0.154±0.007	16/68
	2.5< R_T <5.0	0.486±0.019	58±6	0.176±0.008	0.148±0.010	11/68
Away	0.0< R_T <0.5	0.327±0.041	59±7	0.180±0.007	0.147±0.008	5/68
	0.5< R_T <1.5	0.408±0.017	58±3	0.173±0.003	0.141±0.005	24/68
	1.5< R_T <2.5	0.466±0.016	60±4	0.164±0.005	0.134±0.007	15/68
	2.5< R_T <5.0	0.500±0.015	61±5	0.159±0.007	0.130±0.009	11/68
Transverse	0.0< R_T <0.5	0.280±0.031	63±4	0.148±0.003	0.119±0.004	15/68
	0.5< R_T <1.5	0.391±0.015	62±3	0.156±0.003	0.126±0.004	29/68
	1.5< R_T <2.5	0.466±0.012	61±3	0.159±0.004	0.126±0.006	31/68
	2.5< R_T <5.0	0.508±0.012	63±4	0.157±0.006	0.126±0.008	17/68

the entire event activity range. We show the pull distribution in Fig. 2 to further quantitatively analyze the deviation between the fit and the experimental data. The pull distribution indicates that the deviations are very small, with all deviations constrained within the three sigma lines, and no significant dependence on the region or R_T is observed. Slightly larger deviations in the pull distribution can be observed in the intermediate R_T regions, especially in the transverse region.

We perform the same TBW analysis with an independent baryon non-extensive parameter on the p_T spectra in high energy proton proton collisions categorized by the unweighted transverse spherocity $S_O^{p_T=1}$ in three intervals [26]. The TBW4 fits to the pion, kaon, and proton p_T data in different spherocity bins, and the corresponding pull distributions for the fits are presented in Fig. 3 following the same cosmetics implemented in Figs. 1 and 2. The results are shown for $S_O^{p_T=1}$ within 0−100%, 0−10%, and 90−100% categories from left to right, with p_T spectra at the top and the corresponding pull distributions at the bottom. The spherocity classified events are all selected with a 0−1% mid-rapidity hadron yield. High multiplicity events are often driven by MPI effects. We utilize the spherocity dependent p_T spectra from events in the top 1% of the mid-rapidity track number distributions to identify the connection between the MPI event structure and the flow like features appearing in high multiplicity events [26]. In high multiplicity events, the particle yields shown in Fig. 3 are considerably higher than those shown in Fig. 1. Reasonable descriptions for all spherocity events are obtained in this fit. Larger χ^2 is found for the spherocity separated events, suggesting that these events contain convoluted effects from multiple physics process and thus have larger fluctuations. More details of the fit parameters are presented in Table 2.

In addition, we compare the fits to the events in various flattenicity bins associated with two different event multiplicity classes [39]. The results of p_T spectra and pull distributions for minimum bias events selected with the ALICE V0M detector in 0−100% percentile are shown in Figs. 4 and 5, respectively. Compared to the case using other event shape selectors, p_T spectra classified by the flattenicity measurement can be matched to the TBW distribution at a very high precision level. Agreement between data and theoretical fits is found for each particle species along the entire p_T range for all $1-\rho$ bins. Considering that the flattenicity classifier is more sensitive to the pile up of the MPI process [39], this agreement suggests that the Tsallis distribution is a good approximation to represent the kinematics of a single MPI process. Flattenicity classified high multiplicity events with 0−1% V0M amplitudes are included in this analysis, as shown in Figs. 6 and 7. The experimental data align with the model expectations except for some slightly larger deviations in flattenicity classes from 0−1% to 10%−20% at low p_T, as indicated in Fig. 7. Table 3 includes the values for the key parameters obtained in these fits.

B. Extracted kinetic freeze-out parameters with different event shapes

In this section, we examine the model parameters extracted from the TBW4 fits, including the non-extensive parameter for mesons (q_M) and baryons (q_B), average radial flow velocity in the transverse plane ($\langle\beta\rangle$), and kinetic freeze-out temperature (T). The effective temperature $T_{\rm eff} = \sqrt{\frac{1+\langle\beta\rangle}{1-\langle\beta\rangle}}T$ has also been provided to estimate the combined effect of flow and temperature on p_T. If q approaches unity, the Tsallis distribution of the emitting

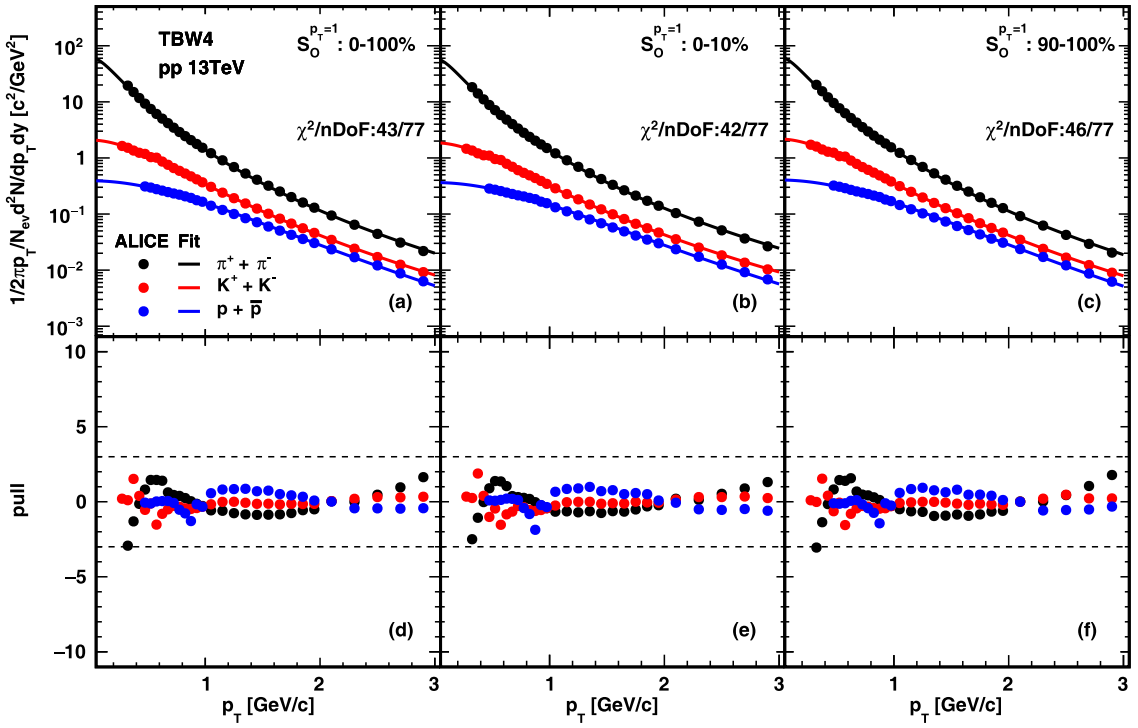

Fig. 2. (color online) Deviations of TBW4 fits to hadron spectra divided by data uncertainties in pp collisions at $\sqrt{s}$ = 13 TeV. Black, red, and blue correspond to π, K, and p particles, respectively. From top to bottom, the rows represent R_T intervals of 0−0.5, 0.5−1.5, 1.5−2.5, and 2.5−5. From left to right, the columns represent the forward, backward, and transverse regions. The dashed lines represent where the difference between the model and experiment data is three times the error of data.

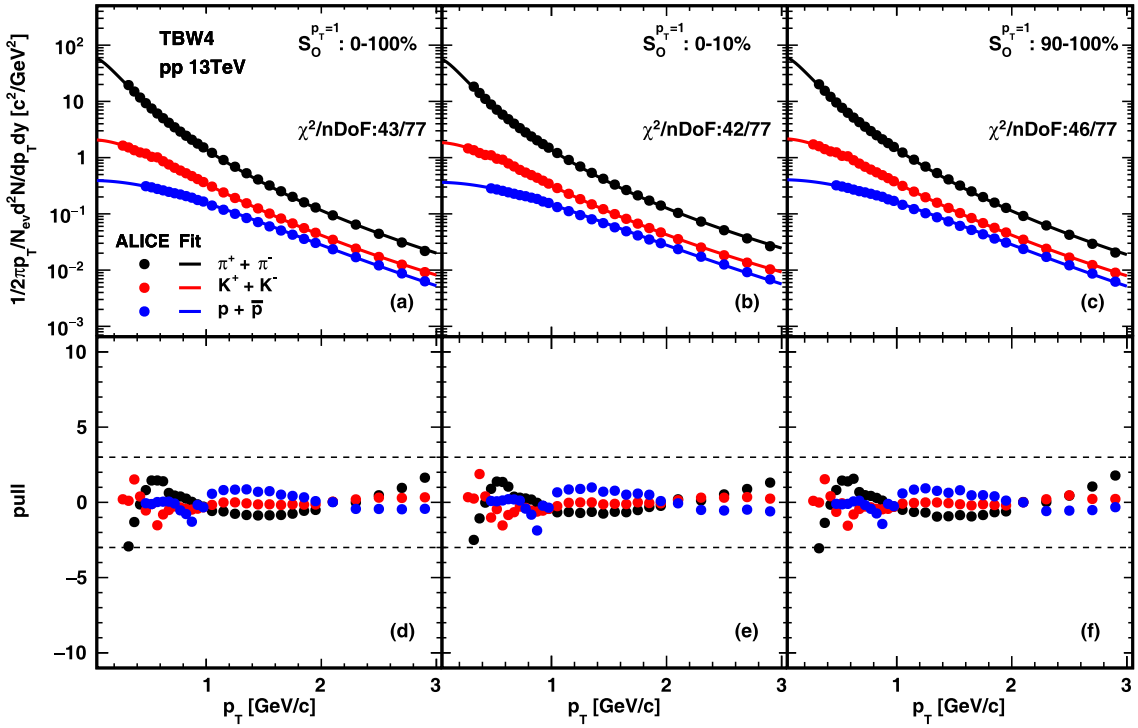

Fig. 3. (color online) TBW4 fits to hadron spectra in pp collisions at $\sqrt{s}$ = 13 TeV. Black, red, and blue correspond to π, K, and p particles, respectively. The points represent the ALICE experimental data [26], and the lines represent the fit results. From left to right, the columns represent sphericity intervals of 0−100%, 0−10%, and 90%−100%. The top row shows the p_T spectra, and the uncertainties in the experimental data are the quadratic sum of statistical and systematic errors. The bottom shows deviations from the p_T fit, and the dashed lines indicate where the difference between the model and experimental data is three times the uncertainty of the data.

Table 2. Extracted kinetic freeze-out parameters and $\chi^2/nDoF$ from TBW4 fits to identified particle transverse spectra in pp collisions at $\sqrt{s}$ = 13 TeV for different $S_O^{pT=1}$ values.

$S_O^{pT=1}$	$\langle\beta\rangle$	T/MeV	q_M-1	q_B-1	$\chi^2/nDoF$
0−100%	0.481±0.009	70±2	0.143±0.003	0.109±0.004	43/77
0−10%	0.477±0.009	64±3	0.157±0.003	0.120±0.004	42/77
90%−100%	0.485±0.008	71±2	0.137±0.003	0.104±0.004	46/77

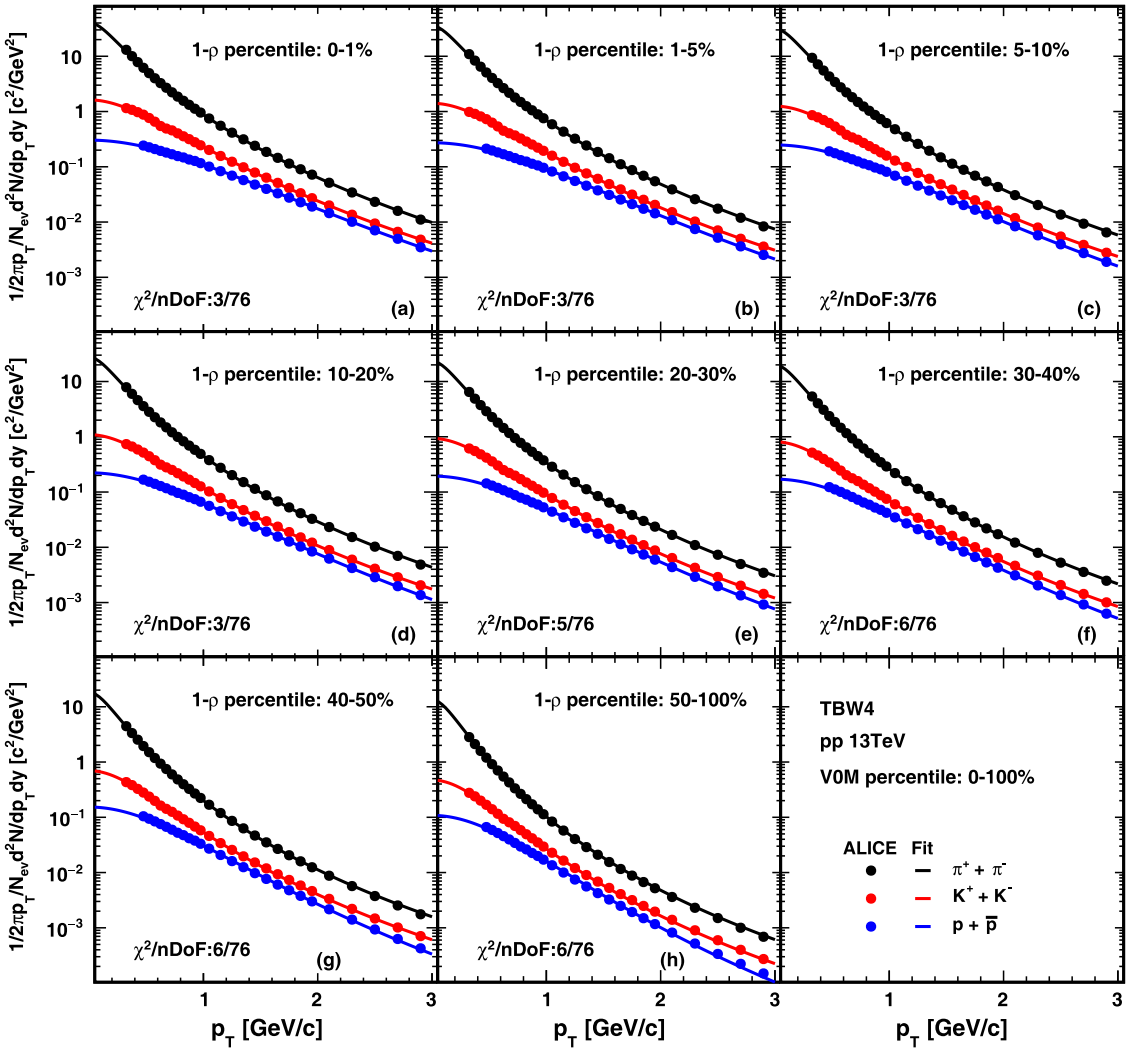

Fig. 4. (color online) TBW4 fits to hadron spectra in pp collisions at $\sqrt{s}$ = 13 TeV. Black, red, and blue correspond to π, K, and p particles, respectively. The points represent the ALICE experimental data [39], and the lines represent the fit results. From panel (a) to (h), the results of different flattenicity event classes for multiplicity-integrated events (V0M percentile 0−100%) are presented. The uncertainties in the experimental data are the quadratic sum of statistical and systematic errors.

source reduces to an exponential thermal distribution, as typically observed in equilibrium systems. The magnitude of q-1 thus serves as a measure to quantify the degree of non-equilibrium effects present in the system. In the following comparisons, we employ the charged particle density information associated with each event shape class and include an event activity like quantity to confront the trend of extracted parameters from different event shape classifiers on the same basis.

$$R_{ch} = \frac{\mathrm{d}N/\mathrm{d}\eta}{\langle \mathrm{d}N/\mathrm{d}\eta \rangle}, \tag{5}$$

where $\mathrm{d}N/\mathrm{d}\eta$ represents the charged particle density at a given event category, and $\langle \mathrm{d}N/\mathrm{d}\eta \rangle$ represents the average charged particle density across all events. In the sub-

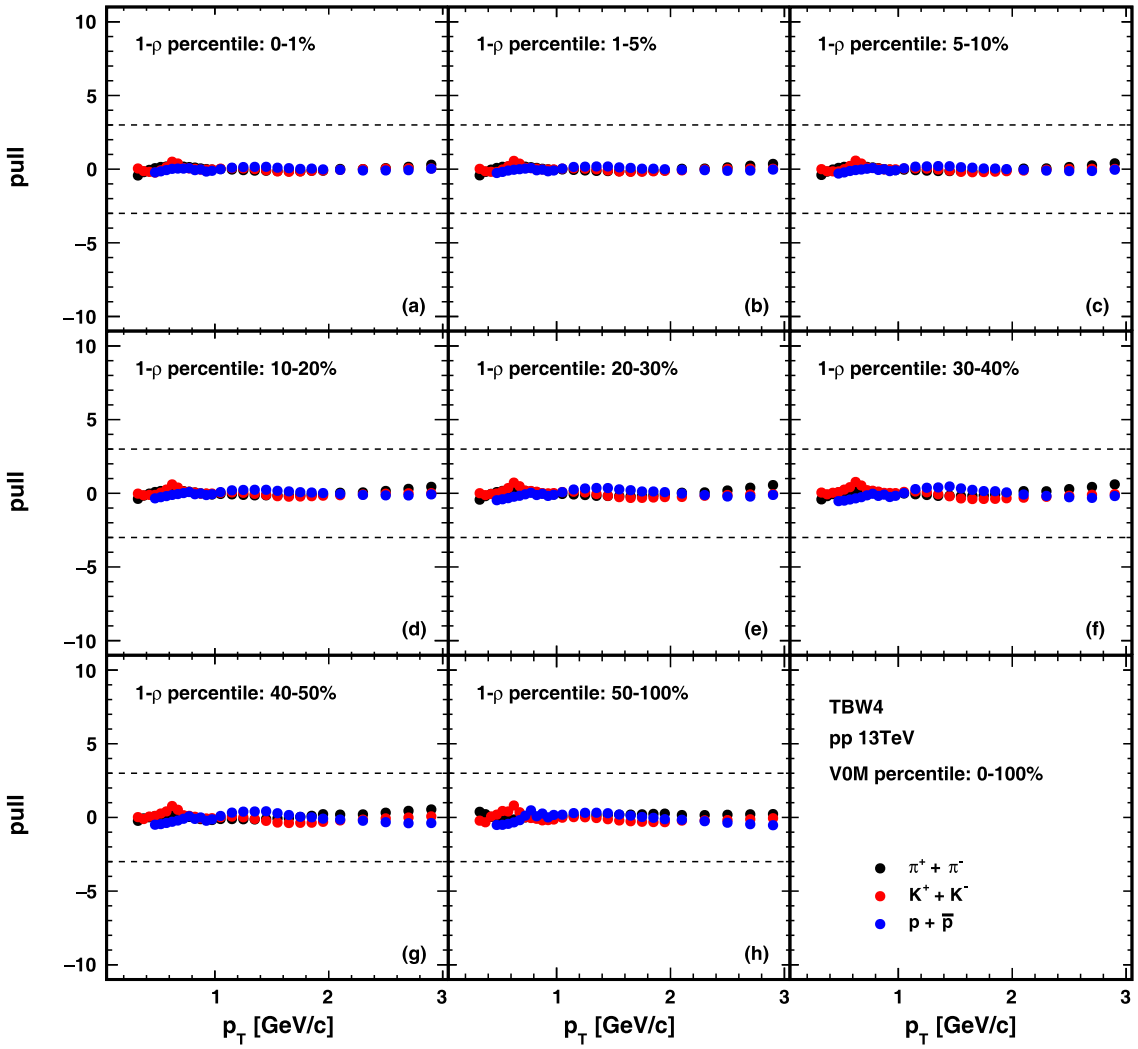

Fig. 5. (color online) Deviations of TBW4 fits to hadron spectra divided by data uncertainties in pp collisions at $\sqrt{s}$ = 13 TeV. Black, red, and blue correspond to π, K, and p particles, respectively. From panel (a) to (h), the results of different flattenicity event classes for multiplicity-integrated events (V0M percentile 0−100%) are presented. The dashed lines represent where the difference between the model and experiment data is three times the error of data.

sequent calculations involving R_{ch}, we use the value of $\langle dN/d\eta \rangle$ = 6.93±0.09 from INEL>0 events at pp 13 TeV [42] to construct this scaling variable.

In Fig. 8, the results for the four parameters obtained with transverse activity classifiers varying with R_T and charged multiplicity classifiers varying with R_{ch} are displayed on the left of the vertical dashed line. The black, red, and blue markers correspond to the results from the toward, away, and transverse regions, respectively. The green markers denote the freeze-out parameters extracted from the inclusive particle p_T spectra classified with event multiplicities obtained from our previous study [29]. The R_T and R_{ch} values for events with different classifiers are within same range 0−4. Further, we show the parameters obtained with the unweighted transverse spheroicity categorizer in the same figures. As those events are selected with the high multiplicity cut, R_{ch} is higher than 4 and the difference between the R_{ch} value of each spherocity bin is considerably small. Therefore, we place the corresponding results at the right of the vertical dashed line in each figure and shift them horizontally with increasing spherocity. The black, red, and blue cross symbols represent the results from the spherocity intervals 0−10%, 0−100%, and 90%−100%, respectively.

The non-extensive parameter values are presented in Fig. 8(a), with solid and open markers representing q_M and q_B, respectively. We observe that both q_M and q_B follow a similar R_T or R_{ch} dependence across all topological regions and event shape estimators. Moreover, a clear hierarchy related to event activity can be found: the non-extensive parameter decreases from the toward region to the transverse region, indicating that non - equilibrium effects are more pronounced in the jet production zones. The transverse region q increases with R_T similar to the

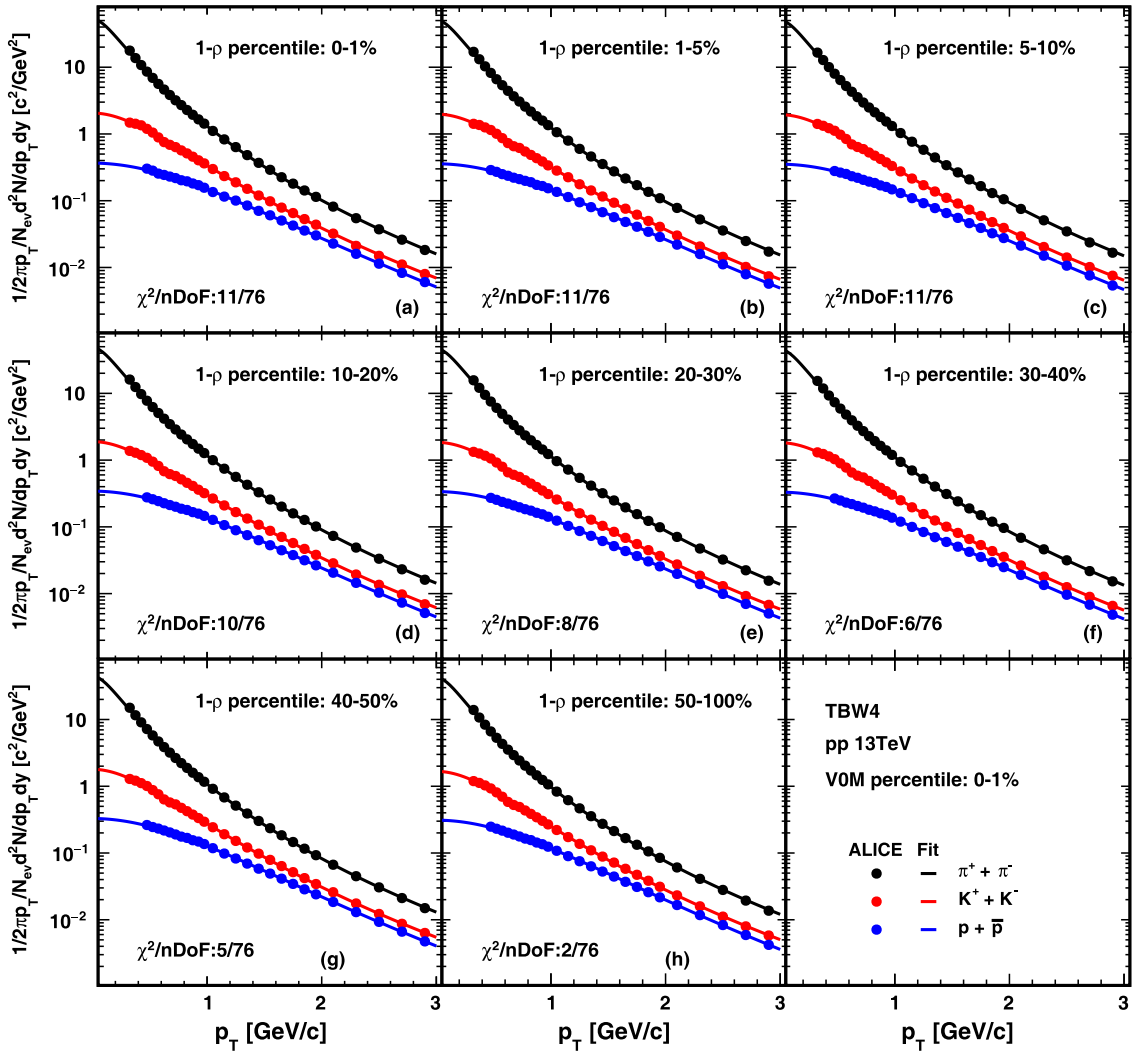

Fig. 6. (color online) TBW4 fits to hadron spectra in pp collisions at $\sqrt{s}$ = 13 TeV. Black, red, and blue correspond to π, K, and p particles, respectively. The points represent the ALICE experimental data [39], and the lines represent the fit results. From panel (a) to (h), the results of different flattenicity event classes for high-multiplicity events (V0M percentile 0−1%) are presented. The uncertainties in the experimental data are the quadratic sum of statistical and systematic errors.

behavior observed for n_{ch} classified events dependent on R_{ch}. Conversely, in the toward and away regions, q exhibits a decreasing trend. However, the q values in different topological regions converge at high R_T with the results from n_{ch} classifier at high R_{ch}, suggesting that the events become isotropic when multiplicity becomes very high and the MPI effects become very important in jet-dominated regions. The decreasing trend in the toward and away regions reflects a competition between non-equilibrium effects and MPI processes, which evolves with increasing event multiplicity.

The freeze-out temperature T, as shown in Fig. 8(b), remains nearly constant for all R_T values in each event topological region despite the substantial uncertainty in fit parameters. The temperature in the toward region is systematically smaller than that in the away and transverse regions. Unlike the n_{ch} classifier, where T decreases with R_{ch}, the temperature extracted by the transverse activity selector is lower, probably because of the $p_T > 5$ GeV/c requirement that is imposed when selecting events based on transverse activity. Thus, it is not surprising to see that the radial flow velocity sensitive to the transverse energy density is significantly higher when using a transverse activity selector compared to the n_{ch} estimator, as shown in Fig. 8(c). The radial flow velocity from different topological regions is close to each other and increases with R_T, which starts from a non-zero value even at low R_T. The effective temperature presented in Fig. 8(d), which encapsulates both thermal motion and collective transverse expansion, increases with rising transverse activity. This trend can be attributed to the rapid growth of radial flow velocity with increasing R_T, indicating that MPI effects play a significant role in shaping transverse momentum spectra across all event topologies.

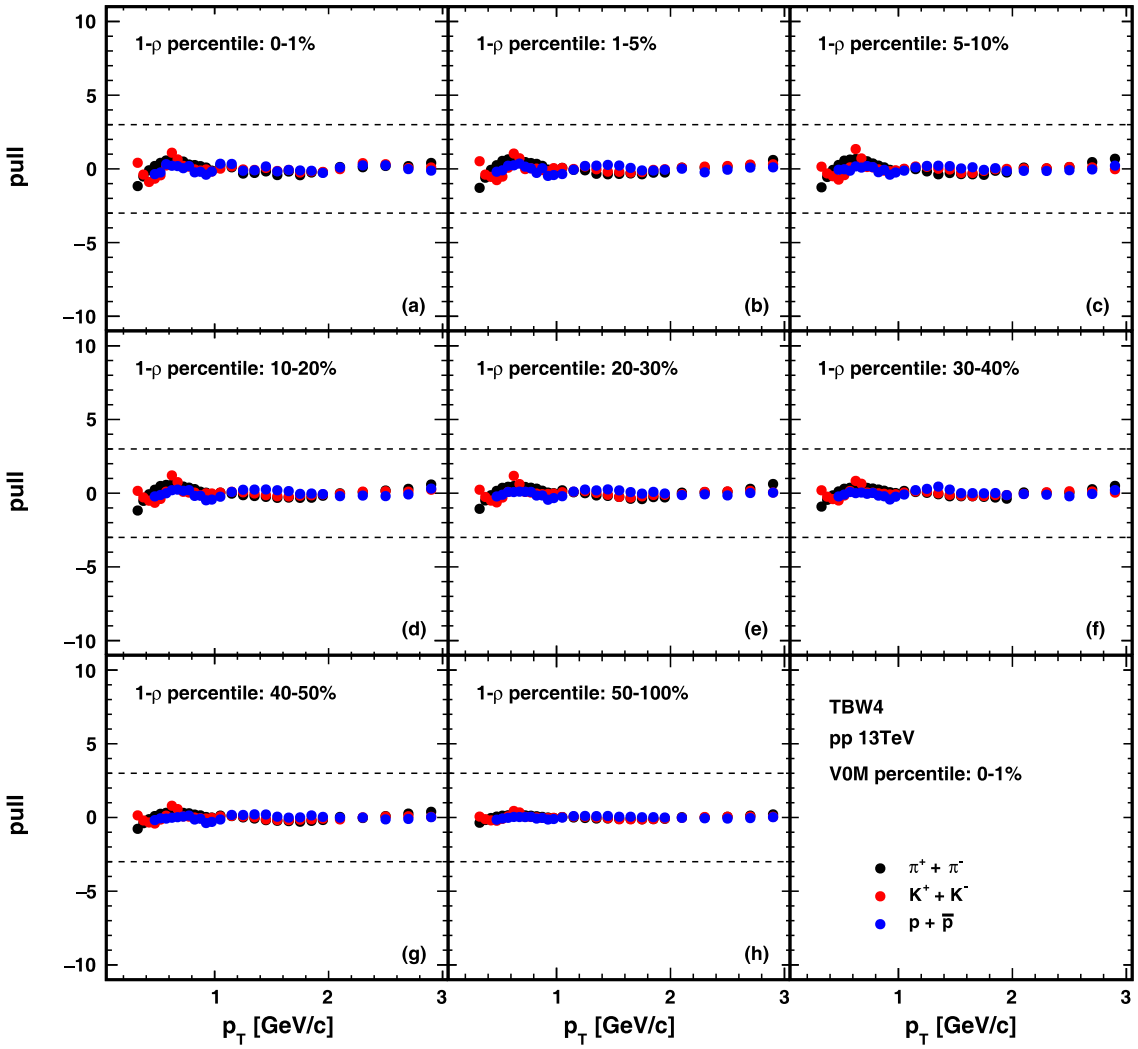

Fig. 7. (color online) The deviations of TBW4 fits to hadron spectra divided by data uncertainties in pp collisions at $\sqrt{s}$ = 13 TeV. Black, red, and blue correspond to π, K, and p particles respectively. From panel (a) to (h), the results of different flattenicity event classes for high-multiplicity events (V0M percentile 0–1%) are presented. The dashed lines represent where the difference between the model and experiment data is three times the error of data.

Applying the spherocity classifier reveals a systematic decline in the Tsallis non-extensivity parameter as one moves from pencil-like events (0−10% spherocity percentile) to sphere-like events (90−100% percentile). q values extracted for sphere-like selections are substantially lower than those obtained via alternative classification methods, which underscore the ability of spherocity to isolate near-equilibrium, isotropic particle distributions. However, the kinetic freeze-out temperature is found to be slightly larger in more isotropic events than that in jetty events. This trend mirrors observations from transverse activity studies, where jet-associated regions show higher q and lower temperatures. The radial flow velocity appears to be insensitive to the spherocity selection and reaches saturation because these events already correspond to high–multiplicity collisions with very large transverse energy density. The effective temperature appears to increase from jetty events to isotropic events because of the enhancement of the kinetic freeze-out temperature rather than changes in flow velocity.

The same kinematic freeze-out parameter distributions obtained for flattenicity estimators are presented in Fig. 9. The results for multiplicity integrated events and 0−1% V0M high multiplicity events are presented with black and red markers, respectively. The results are presented as a function of R_{ch}. Flattenicity grows with an increase in R_{ch}, which indicates that events shift to more uniform distributions. Figure 9(a) shows the non-extensive parameters for meson (q_M) and baryon (q_B) in solid and open markers. The non-extensive parameters remain nearly constant across different flattenicity bins within uncertainties. In addition, the values of q_M and q_B closely match those observed in spherocity identified events with the highest isotropy within the 90−100% $S_O^{p_T=1}$ percentile.

Table 3. Extracted kinetic freeze-out parameters and $\chi^2/nDoF$ from TBW4 fits to identified particle transverse spectra in pp collisions at $\sqrt{s}$ = 13 TeV for different V0M and $1-\rho$ values.

V0M	$1-\rho$	$\langle\beta\rangle$	T/MeV	q_M-1	q_B-1	$\chi^2/nDoF$
0−100%	0-1%	0.447±0.032	79±11	0.129±0.012	0.104±0.013	3/77
	1-5%	0.418±0.034	78±11	0.133±0.011	0.106±0.011	3/77
	5-10%	0.392±0.038	77±11	0.135±0.010	0.108±0.011	3/77
	10-20%	0.361±0.040	77±10	0.136±0.008	0.109±0.009	3/77
	20-30%	0.322±0.036	77±8	0.136±0.006	0.110±0.006	5/77
	30-40%	0.275±0.040	77±7	0.136±0.004	0.111±0.005	6/77
	40-50%	0.228±0.051	73±6	0.140±0.005	0.112±0.006	6/77
	50-100%	0.003±0.064	71±4	0.138±0.004	0.109±0.003	6/77
0−1%	0-1%	0.490±0.014	80±5	0.125±0.006	0.100±0.007	11/77
	1-5%	0.484±0.014	79±5	0.128±0.006	0.103±0.007	11/77
	5-10%	0.481±0.014	78±4	0.129±0.005	0.103±0.006	11/77
	10-20%	0.480±0.014	79±5	0.128±0.006	0.102±0.007	10/77
	20-30%	0.476±0.014	80±5	0.127±0.006	0.102±0.006	8/77
	30-40%	0.472±0.016	81±6	0.127±0.006	0.103±0.007	6/77
	40-50%	0.468±0.019	81±7	0.128±0.007	0.104±0.007	5/77
	50-100%	0.459±0.038	78±14	0.132±0.015	0.106±0.017	2/77

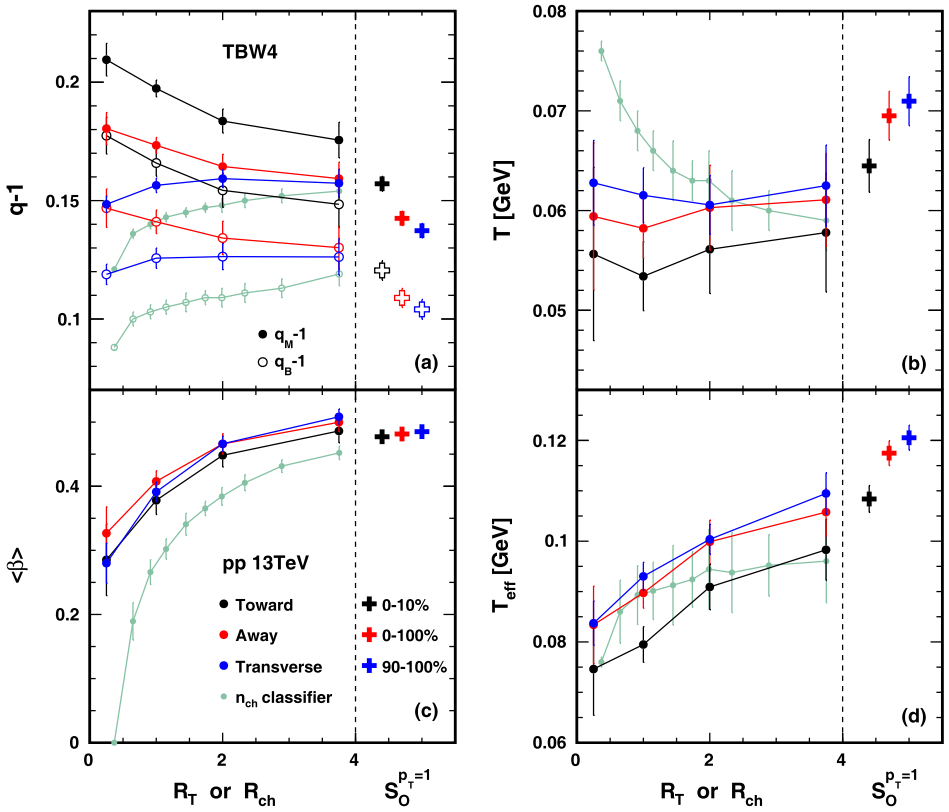

Fig. 8. (color online) R_T, R_{ch}, and $S_O^{p_T=1}$ dependencies of extracted freeze-out parameters and effective temperature $T_{\rm eff}$ in pp collisions at $\sqrt{s}$ = 13 TeV from TBW4 fits. The black, red and blue circle markers correspond to toward, away, and transverse regions. The green circle markers [29] correspond to the n_{ch} classifier. The cross markers correspond to different sphericity. In panel (a), open markers represent the results of q_B-1, and solid markers represent the results of q_M-1.

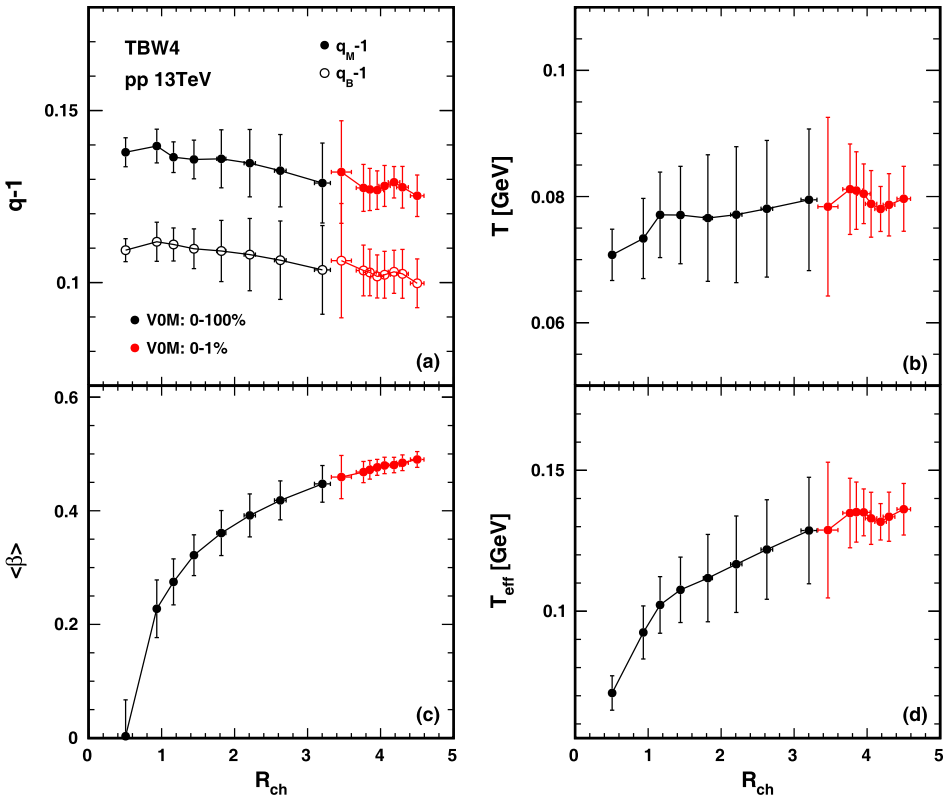

Fig. 9. (color online) R_T dependence of extracted freeze-out parameters and effective temperature $T_{\rm eff}$ in pp collisions at $\sqrt{s}$ = 13 TeV from TBW4 fits. Black and red represent flattenicity in multiplicity-integrated and high-multiplicity event classes. The direction of increasing R_T is consistent with the direction of increasing flattenicity (from 50−100% to 0−1%). In panel (a), open markers represent the results of $q_B - 1$, and solid markers represent the results of $q_M - 1$.

The freeze-out temperature shown in Fig. 9(b) is also flat and close to the value obtained in isotropic events. This value is higher than the temperature extracted from the high multiplicity n_{ch} selected events. As the flattenicity estimator is considered to be less biased toward the high p_T jet effects and focusing on the MPI related soft QCD dynamics, this constancy indicates that hadron productions in pp collisions decouple at similar local statistical freeze-out conditions, regardless of event multiplicity. The radial flow velocity shown in Fig. 9(c) increases with R_{ch} (and with flattenicity) similar to the observation found in general multiplicity or transverse activity estimators. The effective temperature displayed in Fig. 9(d) rises with R_{ch} in multiplicity integrated events, driven by enhanced flow velocity. In high multiplicity events (0−1% V0M selection), the effective temperature remains relatively stable, reflecting minimal variations in p_T spectra with respect to flattenicity [39]. Overall, the flattenicity classifier effectively decouples jet-related hadronization effects reflected in the non-extensive parameter and local temperature from collective flow dynamics driven by stacked MPI processes, thereby providing a clean probe of the soft QCD freeze-out stage.

Determining the onset of collectivity in small systems is crucial for understanding if they can achieve the critical energy density necessary for QGP formation. Such an investigation is conducted using global multiplicity to estimate the energy density of the system. A prominent approach to this search, exemplified by the work of Refs. [43, 44], employed Tsallis and Hagedorn functions to fit the hadron spectrum in pp collisions, identifying an inflection point in the transverse flow velocity as a possible phase transition signal. Their analysis suggests a smooth evolution toward thermalization at high event activity similar to the findings in this study. It is interesting to note that the current study incorporating event shape observables offers a more differential probe of the properties of the medium than multiplicity alone. We argue that the emergence of collective effects is not only dependent on the global energy density probed by multiplicity but also on its spatial distribution within the collision volume. Event shape classifiers enable comparisons between events with similar multiplicities but vastly different internal geometries, providing complementary dimension to works in Refs. [43, 44].

C. Parameter correlation

In the context of non-equilibrium statistics, temperature and flow velocity can be associated with viscosity through linear or quadratic dependencies on the non-ex-

tensive parameter. Figure 10 displays the results of $\langle\beta\rangle$ and T varying with q-1 from TBW4 fits with different event shape estimators in pp collisions at $\sqrt{s} = 13$ TeV. The transverse event activity dependencies in the toward, away, and transverse regions are shown in different colors with the marker styles representing each R_T bin. The spherocity identified results are demonstrated by the crossing markers with colors indicating different spherocity bins. The flattenicity related results are presented in brown with open and solid markers indicating minbias events and 0−1% V0M high multiplicity events. Meanwhile, we plot the n_{ch} classified results for pp collisions at $\sqrt{s} = 13$ TeV and PbPb collisions at $\sqrt{s_{NN}} = 5.02$ TeV from our previous work [29] in the same figure with cyan and magenta symbols to compare the system size effect. The first row shows the radial flow velocity correlation with the non-extensive parameter. The different event topological region results converge from low R_T to high R_T events, implying that the high R_T events from all topological regions are dominanted by the same underlying event effects. However, the results for the transverse region evolve from low q to high q with an increase in flow velocity with R_T, which suggests that the transverse region receives strong fluctuation effects in high activity events, similar to the observations in n_{ch} classified pp collision results. The same enhancement of hard process bias effects in high multiplicity events may apply to both scenarios to account for this similarity. The $\langle\beta\rangle$ versus q correlations in the toward and away regions shift along the opposite direction, leading to smaller q when $\langle\beta\rangle$ in-

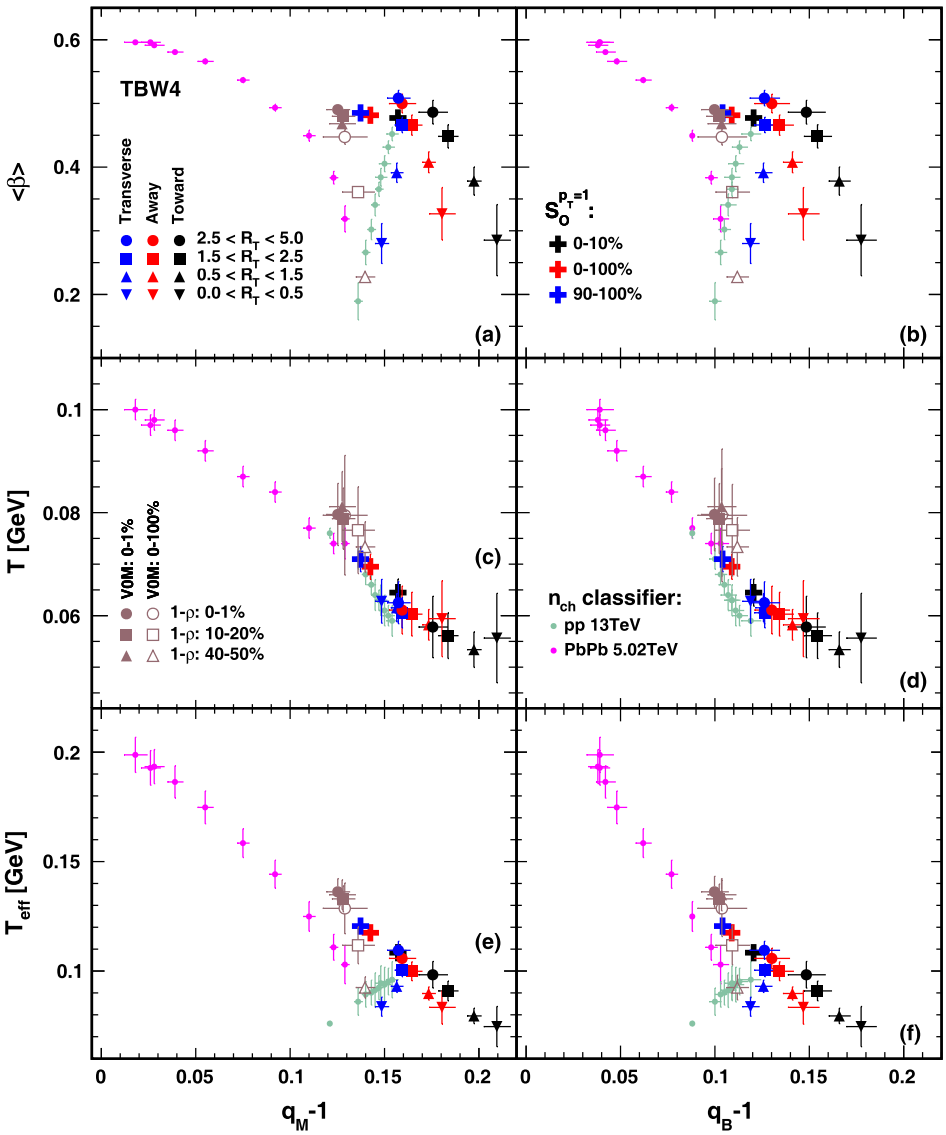

Fig. 10. (color online) $\langle\beta\rangle$ vs. q-1, T vs. q-1, and $T_{\rm eff}$ vs. q-1 in pp collisions at $\sqrt{s}$ = 13 TeV from TBW4 fits. q includes q_M (left column) and q_B (right column). The results for transverse event activity, spherocity, flattenicity, and n_{ch} classifier are shown, with different colors and shapes denoting various event classes. The n_{ch} classifier results are taken from our previous work [29].

creases, which can be understood as an outcome of the interplay between the hard process and underlying event soft physics varying with event activity. The spherocity classified events are restricted to high multiplicity events, and therefore, $\langle\beta\rangle$ remains almost unchanged at a velocity as high as that in the high R_T events while q_M and q_B reduces from azimuthally jetty events (0−10%) to more isotropic events (90−100%) approaching equilibrium. The flattenicity categorized events are found to be only changing in $\langle\beta\rangle$ with the non-extensive parameters being stable with an increase in the flatness of the system. The behavior of the flattenicity driven evolution effects in pp collisions aligns with the large system PbPb collision results.

The kinetic freeze-out temperature correlation with the non-extensive parameter is shown in the second row. A significant universal scaling feature is observed across different collision systems with various event shape categorizers. This universal evolution curve in the T vs q-1 plane reinstates our previous finding of the existence for the universality in the kinetic freeze-out features independent of the collision system, which implies that a unified partonic evolution stage, where similar QCD dynamics govern parton interactions and evolution, leads to consistent freeze-out parameters. The $1-\rho$ identified events have the largest T with very small variations between different flattenicities. The jet induced effects amplified by the toward and away event topological selections for different event activities deliver very small T and large q representing strong dynamical fluctuations in temperature because of hard process effects. The low R_T toward region approaches very small T with large q.

In the third row, we present the effective temperature versus q correlations. A universal upper boundary determined by the maximum radial flow velocity with variations related to the temperature can be found from central PbPb collisions with the largest $T_{\rm eff}$ and smallest q to the jetty toward region results with the smallest $T_{\rm eff}$ and largest q. The diverged radial flow velocity dependence in each event shape selection leads to evolutions along different branches under the common boundary because of the energy density constrained by the system size.

This comparison reveals that the statistical freeze-out parameter space is largely expanded with different event shape measurements. Event shapes can tag the different limits of the freeze-out parameter space for pp collisions. Further, there is a maximum kinetic freeze-out temperature and flow velocity that can be reached in pp collisions with all different event shapes at a level close to the peripheral PbPb collisions. This difference represents the enhancement of inter-nucleon dynamics in generating the initial energy and entropy densities compared to the sub-nucleon partonic fluctuations induced by color glass condensate effects. In all these different event shape observables, the flattenicity shows unique features of mimicking the collective motion effects observed in PbPb collisions by overlapping multiple parton interactions in an additive way, thereby making this observable of special interest to isolate the soft interaction dominated flow physics in small systems.

IV. SUMMARY

In this study, we employed the TBW4 model with the independent baryon non-extensive parameter q_B to fit the p_T spectra of π, K, and p in $\sqrt{s}=13$ TeV pp collisions with different event shapes. Utilizing event shape classifiers including transverse event activity, unweighted transverse spherocity, and flattenicity, we explored the connection between event shape and particle emission characteristics in pp collisions. Across all classifiers and topological regions, TBW4 describes the spectra relatively well, even when selecting events with a high p_T leading track in event activity studies.

The non-extensive parameters decrease with increasing isotropy or MPI activity, indicating that more isotropic, MPI-dominated events approach equilibrium. A stronger fluctuation effect caused by the nonequilibrium dynamics represented by the magnitude of the nonextensive parameter is found in the toward and away regions compared to the transverse region results. The radial flow velocity increases with the activity or multiplicity of the event in all different topological regions of the event with various event shapes, and it saturates in high-multiplicity bins, reflecting stronger collective expansion in denser underlying events. Freeze-out parameter values from different event topological regions relative to the leading particle converge at high activity, indicating a common soft-physics limit across topologies. Although the kinetic freeze-out temperature T shows less variation across event classes, a universal scaling in the T vs q-1 plane is observed, which is consistent with previous findings and demonstrates a common freeze-out physics governed by entropy production and multi-parton interactions [29]. Comparisons with PbPb collisions highlight similarities in the maximum achievable collective effects in pp events and peripheral heavy-ion collisions. The flattenicity classifier effectively decouples jet-related hadronization effects and local temperature from collective flow dynamics, providing a cleaner probe of the soft QCD freeze-out stage. The non-extensive parameters and freeze-out temperature remain nearly constant across different flattenicity bins, similar to the values in highly isotropic spherocity identified events.

The study explores the interplay of hard partonic scattering and soft processes during the development of flow-like signatures. These findings highlight the effectiveness of event shape classifiers in probing soft QCD processes and collective phenomena in small systems,

thereby providing valuable insights into the emergence of collective phenomena and the nature of the freeze-out stage in high-energy proton-proton collisions.

ACKNOWLEDGMENTS

We would like to thank Zebo Tang, Wangmei Zha, and Qiye Shou for helpful discussions.

References

[1] W. Broniowski, M. Chojnacki, W. Florkowski *et al.*, Phys. Rev. Lett. **101**, 022301 (2008), arXiv: 0801.4361[nucl-th]
[2] H. Elfner and B. Müller, J. Phys. G **50**, 103001 (2023)
[3] J. W. Harris and B. Müller, Eur. Phys. J. C **84**, 247 (2024)
[4] U. W. Heinz, Landolt-Bornstein **23**, 240 (2010)
[5] C. Gale, S. Jeon, and B. Schenke, Int. J. Mod. Phys. A **28**, 1340011 (2013)
[6] F. Retiere and M. A. Lisa, Phys. Rev. C **70**, 044907 (2004)
[7] E. Schnedermann, J. Sollfrank, and U. W. Heinz, Phys. Rev. C **48**, 2462 (1993)
[8] E. Schnedermann and U. W. Heinz, Phys. Rev. C **50**, 1675 (1994)
[9] U. W. Heinz, arXiv: hep-ph/0407360
[10] J. Chen *et al.*, Nucl. Sci. Tech. **35**, 214 (2024)
[11] Q.-Y. Shou *et al.*, Nucl. Sci. Tech. **35**, 219 (2024)
[12] J. L. Nagle and W. A. Zajc, Ann. Rev. Nucl. Part. Sci. **68**, 211 (2018)
[13] J. Adolfsson *et al.*, Eur. Phys. J. A **56**, 288 (2020)
[14] J. Noronha, B. Schenke, C. Shen *et al.*, Int. J. Mod. Phys. E **33**, 2430005 (2024)
[15] T. Sjostrand and P. Z. Skands, JHEP **03**, 053 (2004)
[16] D. d'Enterria, G. K. Eyyubova, V. L. Korotkikh *et al.*, Eur. Phys. J. C **66**, 173 (2010)
[17] S. Acharya *et al.* (ALICE), Phys. Lett. B **843**, 137649 (2023)
[18] S. Acharya *et al.* (ALICE), Phys. Rev. C **99**, 024906 (2019)
[19] T. Martin, P. Skands, and S. Farrington, Eur. Phys. J. C **76**, 299 (2016)
[20] S. Acharya *et al.* (ALICE), JHEP **06**, 027 (2023)
[21] A. Banfi, G. P. Salam, and G. Zanderighi, JHEP **06**, 038 (2010)
[22] B. Abelev *et al.* (ALICE), Eur. Phys. J. C **72**, 2124 (2012)
[23] S. Acharya *et al.* (ALICE), Eur. Phys. J. C **79**, 857 (2019)
[24] A. Ortiz, A. Khuntia, O. Vázquez-Rueda *et al.*, Phys. Rev. D **107**, 076012 (2023)
[25] A. Ortiz, Adv. Ser. Direct. High Energy Phys. **29**, 343 (2018)
[26] S. Acharya *et al.* (ALICE), JHEP **05**, 184 (2024)
[27] S. Acharya *et al.*, arXiv: 2411.09334 [nucl-ex]
[28] Z. Tang, Y. Xu, L. Ruan *et al.*, Phys. Rev. C **79**, 051901 (2009)
[29] L. Liu, Z.-B. Yin, and L. Zheng, Chin. Phys. C **47**, 024103 (2023)
[30] G. Wilk and Z. Wlodarczyk, Phys. Rev. Lett. **84**, 2770 (2000)
[31] G. Wilk and Z. Wlodarczyk, Eur. Phys. J. A **40**, 299 (2009)
[32] J. Chen, J. Deng, Z. Tang *et al.*, Phys. Rev. C **104**, 034901 (2021)
[33] G. Che, J. Gu, W. Zhang *et al.*, J. Phys. G **48**, 095103 (2021)
[34] J. Gu, C. Li, Q. Wang *et al.*, J. Phys. G **49**, 115101 (2022)
[35] S. Prasad, B. Sahoo, S. Tripathy *et al.*, Phys. Rev. C **111**, 044902 (2025)
[36] T. Affolder *et al.* (CDF), Phys. Rev. D **65**, 092002 (2002)
[37] T. Sjostrand and M. van Zijl, Phys. Rev. D **36**, 2019 (1987)
[38] E. Abbas *et al.* (ALICE), JINST **8**, P10016 (2013)
[39] S. Acharya *et al.* (ALICE), Phys. Rev. D **111**, 012010 (2025)
[40] K. Jiang, Y. Zhu, W. Liu *et al.*, Phys. Rev. C **91**, 024910 (2015)
[41] A.-G. Zhang, X.-Y. Peng, X. Peng *et al.*, Nucl. Sci. Tech. **36**, 134 (2025)
[42] S. Acharya *et al.* (ALICE), Eur. Phys. J. C **81**, 630 (2021)
[43] K. K. Olimov, F.-H. Liu, K. A. Musaev *et al.*, Int. J. Mod. Phys. A **36**, 2150149 (2021)
[44] K. K. Olimov, F.-H. Liu, K. A. Musaev *et al.*, Universe **8**, 174 (2022)